Eur. Phys. J. E (2019) **42**: 83
DOI 10.1140/epje/i2019-11838-3

THE EUROPEAN PHYSICAL JOURNAL E

Regular Article

A comparison of ion channel current blockades caused by individual poly(ethylene glycol) molecules and polyoxometalate nanoclusters*

Haiyan Wang[1,2], John J. Kasianowicz[1,3,a], Joseph W.F. Robertson[1], Dianne L. Poster[4], and Jessica Ettedgui[1,5]

[1] National Institute of Standards and Technology, Physical Measurement Laboratory, Gaithersburg, MD 20899, USA
[2] Shenzhen Key Laboratory of Biomedical Engineering, School of Medicine, Shenzhen University, 3688 Nanhai Road, Shenzhen 508060, China
[3] Columbia University, Department of Applied Physics Applied Mathematics, New York, NY 10027, USA
[4] National Institute of Standards and Technology, Material Measurement Laboratory, Gaithersburg, MD 20899, USA
[5] Columbia University, Department of Chemical Engineering, New York, NY 10027, USA

Received 12 September 2018 and Received in final form 22 April 2019
Published online: 28 June 2019

In Memory of Professor Loïc Auvray.

We dedicate this paper to the memory of Professor Loïc Auvray, who was a true gentleman and a renowned scholar. Loïc always asked many questions that probed the heart of the problem of how polymers interact with protein ion channels, and he led a pioneering, world-class research program to investigate those issues. Loïc was also an indispensable, enthusiastic advocate for his young colleagues, and an exceptional mentor to generations of students. He was a friend and colleague of ours at NIST and will be sorely missed.

Abstract. Proteinaceous nanometer-scale pores have been used to detect and physically characterize many different types of analytes at the single-molecule limit. The method is based on the ability to measure the transient reduction in the ionic channel conductance caused by molecules that partition into the pore. The distribution of blockade depth amplitudes and residence times of the analytes in the pore are used to physically and chemically characterize them. Here we compare the current blockade events caused by flexible linear polymers of ethylene glycol (PEGs) and structurally well-defined tungsten polyoxymetallate nanoparticles in the nanopores formed by *Staphylococcus aureus* α-hemolysin and *Aeromonas hydrophila* aerolysin. Surprisingly, the variance in the ionic current blockade depth values for the relatively rigid metallic nanoparticles is much greater than that for the flexible PEGs, possibly because of multiple charged states of the polyoxymetallate clusters.

Introduction

Protein ion channels are nanometer-scale pores that enable a wide range of cellular and intracellular functions [1–3]. They recently have been used to detect and characterize single molecules [4] including ions [5–7], RNA and DNA oligonucleotides [8,9], synthetic polymers [10–16], and unfolded proteins [17]. They are also the basis of two new DNA sequencing devices [8,14,18–20], provide the ability to separate polymers based on their size [14–16], and are used to estimate the energies (or forces) of intermolecular interactions [21–24]. This analytical capability was made possible by modifying the natural behavior of protein ion channels and taking advantage of how molecules interact with them (*i.e.*, the channels remain open indefinitely [5, 6,25] and the molecules of interest bind reversibly to the pore walls) [4,11].

In the method of nanopore-based sensing, a single molecule that enters the pore causes a transient decrease in the ionic current, in part due to volume exclusion [14, 15]. However, the binding of mobile ions (*e.g.*, K^+) to single molecules, such as polymers of ethylene glycol (PEGs),

* Contribution to "Polymers: From Adsorption to Translocation - Topical Issue in Memoriam Loïc Auvray (1956–2016)" edited by Jean-Marc Di Meglio, Fabien Montel, Jan C. Behrends.

[a] e-mail: john.kasianowicz@nist.gov

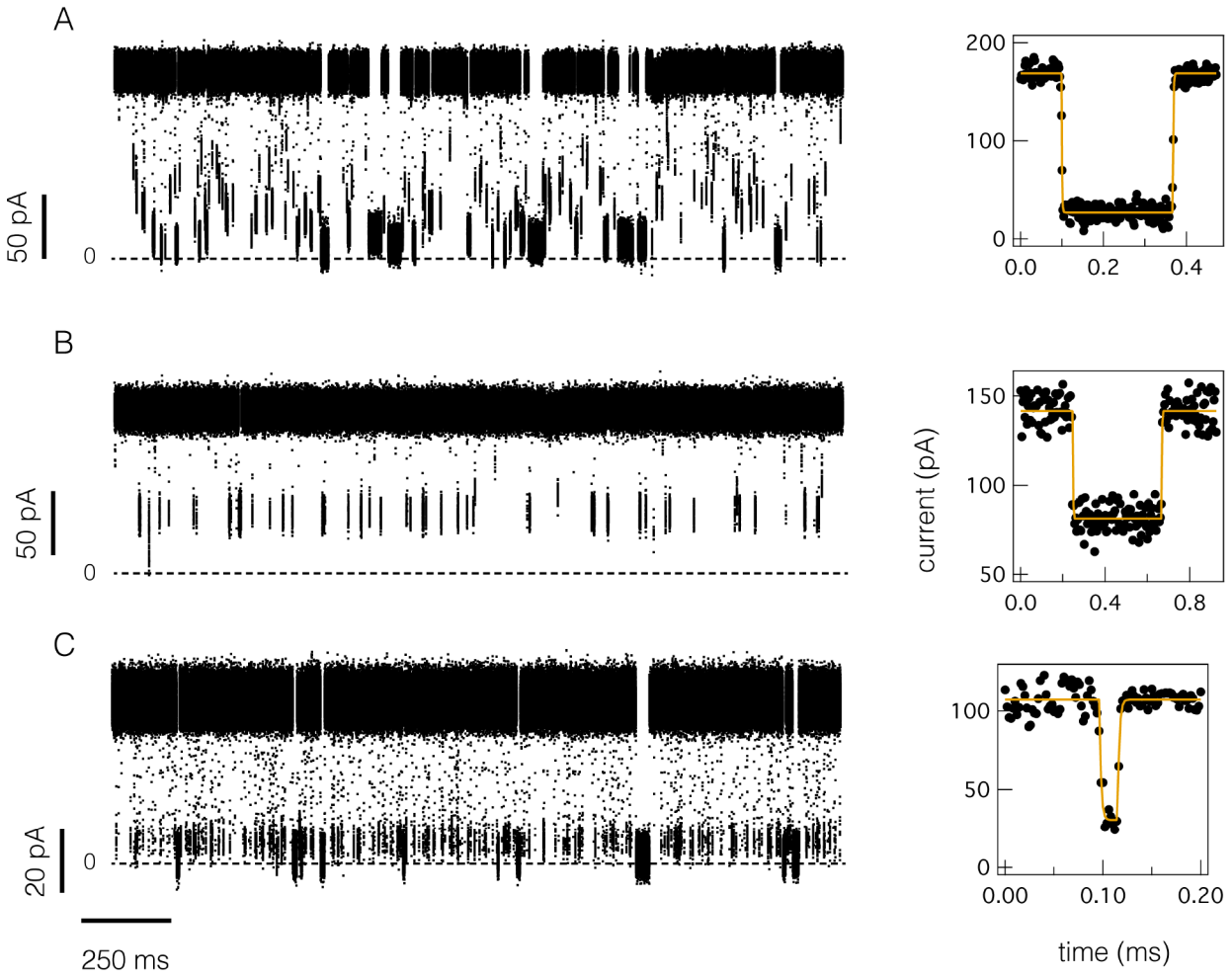

Fig. 1. Different ionic current blockade patterns in single αHL ion channels caused by polymers of ethylene glycol (PEG), and metallic nanoparticles. Ionic current blockade events are due to (A) nonuniform PEGs with mean molecular masses $Mw = 1000$, 2000, and 3000 g/mol, and a chemically purified uniform PEG29 ($Mw = 1294$ g/mol, 4 M KCl, pH 7.2, and $V = +50$ mV), (B) the chemically purified PEG29 (4 M KCl, pH 7.2, and $V = +50$ mV), and (C) metallic nanoparticles (polyoxomethalates) (1 M NaCl, pH 5.5, and $V = -120$ mV). The right panels show that typical current blockades for each of the three types of molecules are unimodal.

can also reduce the pore conductance, even though the dissociation constant for that interaction is weak ($K_d < 1$ M) [15,25]. That effect is made possible because the mean time a mobile K^+ ion which binds to a PEG polymer ($\langle\tau\rangle \approx 1/k_{off} = K_d/k_{on}$) is comparable to its transit time through the pore [25].

Recently, we demonstrated that nanometer-scale metallic particles, *i.e.*, anionic metal oxygen clusters (polyoxometalates, POMs) [26,27], can be physically characterized by the ion channel formed by *Staphylococcus aureus* alpha hemolysin (αHL) [28]. Specifically, the nanopore-based sensing method was used to measure the pH-dependent changes to various POM species and to discriminate between two subtly different POM isomers. Interestingly, this work also showed that the variance in the ionic current blockade values for POMs is much greater than that for flexible PEG polymers. Here, we try to further explore the basis for that finding and discuss its implications for understanding what the method measures.

Materials and methods

Nonuniform poly(ethylene glycol) ($H(OCH_2CH_2)_nOH$) (Fluka, Lake Ronkonkoma, NY) and a chemically purified sample of uniform PEG ($Mw = 1.294$ g/mol) (Polypure, Oslo, Norway) were used without further processing. POMs were synthesized by adding phosphotungstic acid hydrate, $H_3(P(W_3O_{10})_{4x}H_2O$, CAS number 12501-23-4, Sigma-Aldrich) to deionized water (Millipore, Billerica, MA) containing 1 M or 3 M NaCl buffered with sodium phosphate monobasic (NaH_2PO_3) titrated to pH 5.5 [28].

Planar lipid bilayer membranes (1,2-diphytanoyl-sn-glycero-3-phosphocholine; DPhPC; Avanti Polar Lipids, Alabaster, AL) were formed either on quartz nanocapillaries (Electronic BioSciences, San Diego, CA, herein referred to as EBS) [28,29] or $\approx 50\,\mu$m diameter holes in a MECA-16 microelectrode cavity array chip (Ionera, Freiburg, Germany). αHL (or aerolysin) added to the *cis* side of the chamber spontaneously binds to the membrane and forms

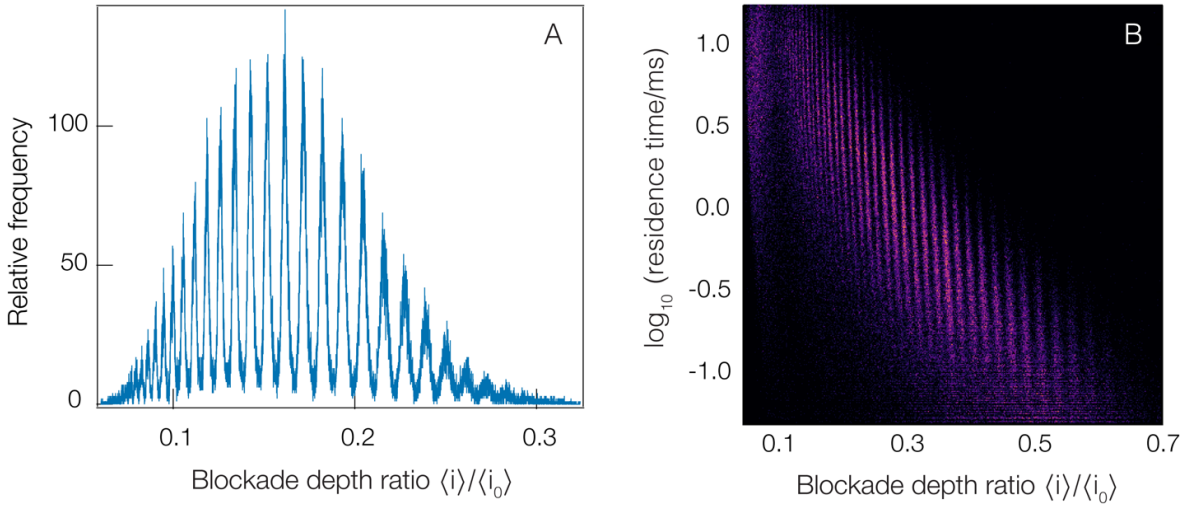

Fig. 2. Nanopore-based single-molecule "mass spectrometry" with a single αHL ion channel. The ability of a nanopore to discriminate between molecules based on their physical (size) and chemical (cation binding) properties. (A) Distribution of the ionic current blockade depth ratio, $\langle i\rangle/\langle i_0\rangle$ for nonuniform PEG with a mean molecular mass $Mw = 1500$. (B) Plot of the event lifetime-relative current blockade depths for a mixture of nonuniform PEGs with mean molecular masses $Mw = 1000$, 2000, and 3000 g/mol. The solution contains 4 M KCl and the applied potential is $V = +50$ mV.

single nanometer-scale pores. PEGs or POMs are added to the *cis* side of the nanopores, and a positive applied potential drives cations from the *cis* to the *trans* side.

Nanopores are formed with either wild-type αHL heptamer [20] or *Aeromonas hydrophila* aerolysin [30–33]. The ionic current through the nanopores is converted to voltage and digitized with either a single EBS FET patch clamp amplifier (for the EBS quartz nanocapillary instrument) or up to eight EBS amplifiers in a custom Nanion Orbit 16 automated parallel bilayer platform [34] (Nanion Technologies, Munich, Germany).

Results and discussion

Ionic current blockades caused by nonelectrolyte linear polymers and metallic nanoparticles

Figure 1 shows representative ionic current blockades caused by the reversible partitioning of PEGs or tungsten-nanoparticle POMs into single αHL ion channels. Nonuniform PEG-induced events (fig. 1(A)) vary in blockade depth because different size polymers reduce the pore conductance to different degrees [14,15,35]. In contrast, the current blockades caused by uniform PEG (fig. 1(B)) or two species of POMs ($[P_2W_5O_{23}]^{6-}$) and $[PW_{11}O_{39}]^{7-}$ [28] (fig. 1(C)) are more uniform in depth. The single-event time series on the right panels of fig. 1(A)–(C) demonstrate that typical blockades caused by each of these types of molecules are unimodal.

Discrimination of polymers at high resolution

Nanopores have been used to identify polymers of PEG based on their molecular mass [14,15,36,37], a method coined as single-molecule "mass spectrometry". Specifically, this technique discriminates between the polymers based on their hydrodynamic radii (*i.e.*, volume exclusion) and the interactions between polymers and mobile ions in the electrolyte solution. With the latter effect, PEGs act as an immobile cation buffer, thereby reducing the effective diffusion coefficient of K^+ and thus the pore conductance (see [15,25,38]). With this technique, PEGs are separated to better than the monomer limit of 44 g/mol (the resolution is ≈ 4 g/mol at $\approx 1,500$ g/mol, see fig. 2(A)). Moreover, the mean residence times of PEGs in an αHL nanopore correlate with the blockade depth ratio $\langle i\rangle/\langle i_0\rangle$ (where $\langle i\rangle/\langle i_0\rangle = 0$ and 1 correspond to a fully blocked and fully open pore, respectively). Control experiments with uniform PEGs confirmed that larger polymers both reduce the pore conductance more, and spend more time on average in the pore, than do smaller ones [14,15].

We developed a physical and chemical theory to describe and ultimately predict at high accuracy this behavior for flexible polymers [15] to advance the application of the nanopore-based analytical method. The question remained whether that theory is generally applicable to other nanopore-particle systems, which we address in part here.

Comparison of PEG- and POM-induced ionic current blockades

Tungsten POMs form multiple species in aqueous solution, and the relative abundance of each depends on the aqueous solution conditions (see [28] and references within). A histogram of ionic current blockades caused by POMs (fig. 3, orange) demonstrate that there are two principal species present at *p*H 5.5, as was expected based on ^{31}P NMR experiments [28,39,40]. Metallic nanoparticles are

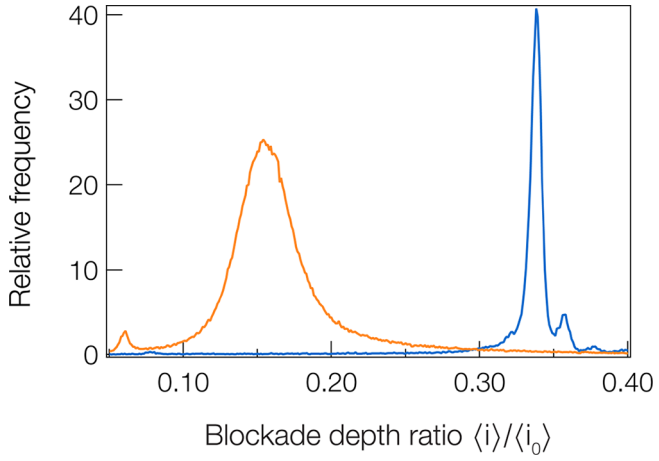

Fig. 3. Histograms of ionic current blockade depth ratios caused by POMs (orange) and purified uniform PEG29 ($Mw =$ 1294 g/mol, blue) in single αHL ion channels. There are two POM species present (in 1 M NaCl, pH 5.5; $V = -120$ mV) due to the $[P_2W_5O_{23}]^{6-}$ and $[PW_{11}O_{39}]^{7-}$ (which we attribute to the peaks at $\langle i\rangle/\langle i_0\rangle \approx 0.03$ and 0.16, respectively). The minor peaks in the PEG data (4 M KCl, pH 7.2, $V = +40$ mV) are caused by trace amounts of smaller PEGs that were not removed in the manufacturer's purification process.

well-defined and presumably rigid structures. Therefore, the variance in the ionic current blockade values for a given species are expected to be relatively small [41], compared to values resulting from flexible polymers such as PEG29 (fig. 3, blue). However, the full-width at half maximum of the current blockade histogram for the POM species' major peak due to $[PW_{11}O_{39}]^{7-}$ (*i.e.*, at $\langle i\rangle/\langle i_0\rangle \approx 0.16$) is 5-fold greater than that of PEG29 polymer (fig. 3) and 12-fold greater than that of PEGs terminated with other moieties [42].

It is conceivable that there are multiple sub-species of different POMs that contribute to that peak width [28]. A plot of the residence time and blockade depth ratio for each event caused by POMs and PEG29 (fig. 4) provides some evidence for that hypothesis. Specifically, as the applied potential decreases ($V = -120$ mV, -100 mV, and -80 mV, figs. 4(A), (B), and (C), respectively), the major POM-induced peak splits into at least two narrower peaks. For comparison, an event-plot analysis of the uniform PEG29 sample ($V = +40$ mV, the opposite polarity used for POMs, because nonelectrolyte PEGs weakly coordinate with mobile cations in solution) is shown in fig. 4(D), it is narrow and discrete, as expected for a predominately uniform species.

It is again tempting to speculate that the multiple peaks in the rightmost part of the POM residence time-blockade event histogram (fig. 4(C)) are due to different sub-species of $[PW_{11}O_{39}]^{7-}$, perhaps those with different amounts of Na^+ ions associated with them [28]. The two apparent peaks for the putative $[PW_{11}O_{39}]^{7-}$ form of the POMs differ by ≈ 0.02, and the POM residence time distributions for the two (or more) slightly separated peaks are not significantly different based on the similarities between their peak heights and widths.

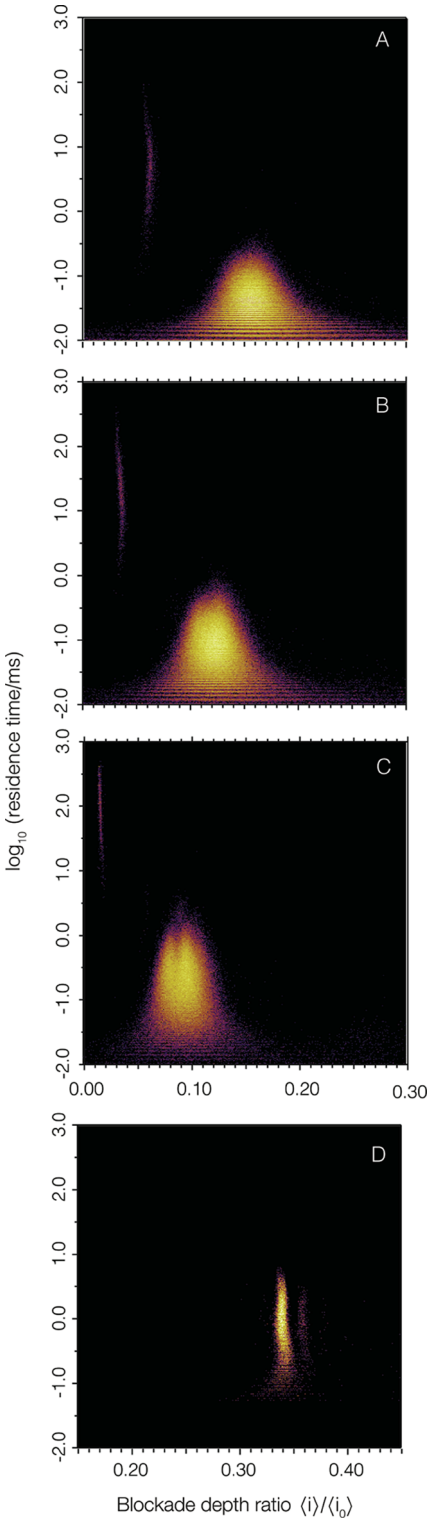

Fig. 4. Comparison of event plots of ionic current blockade depths in single αHL ion channels caused by metallic nanoparticles and flexible polymers of uniform PEG29 ($M_w =$ 1294 g/mol). Plots of the resident time and relative current blockade depths for POMs at $V =$ (A) -120 mV, (B) -100 mV, and (C) -80 mV (1 M NaCl, pH 5.5) and for (D) PEG29 (4 M KCl, pH 7.2; $V = +40$ mV). The data was acquired with an EBS nanocapillary apparatus and EBS field effect transistor amplifier.

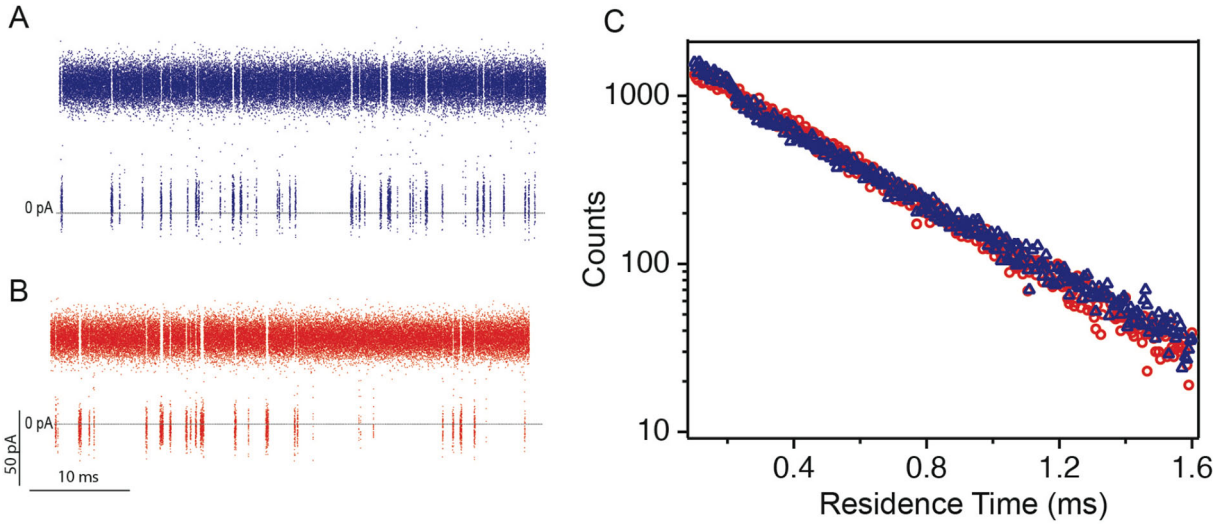

Fig. 5. POMs partitioning into two different nanopores. POMs added to the *cis* side of αHL (A) and aerolysin (B) nanopores cause transient blockades in the ionic current. (C) Residence time distributions for POMs in the αHL (blue triangles) and aerolysin (red circles) nanopores in a log-linear plot. The membranes are formed on $\approx 50\,\mu$m diameter MECA-16 chips in a custom Nanion Orbit 16 system outfitted with 8 EBS FET amplifier headstages. The concentration of POMs in the *cis* chamber is $20\,\mu$M, the applied potential is $V = -40\,$mV and the solutions contain 3 M NaCl buffered at *p*H 5.5.

Based on a comparison of the ^{31}P NMR and nanopore data [28], the leftmost minor peak distribution in figs. 4(A)–(C) (*i.e.*, $\langle i\rangle/\langle i_0\rangle \lesssim 0.06$), is likely due to the $[P_2W_5O_{23}]^{6-}$ species. If that is true, perhaps the blockade depth distributions of each POMs species could be as narrow as those resulting from the PEGs interacting with the pore. Interestingly, this species appears to reduce the ionic current blockade more than does the $[PW_{11}O_{39}]^{7-}$ species.

We speculate that there could be up to seven differently charged subspecies of $[PW_{11}O_{39}]^{7-}$ with different amounts of Na^+ ions ionically bound to them and that the energy barriers for the entry of each into the αHL pore are different. For example, at $V = -120\,$mV, it is clear there is only one wide peak in the event-plot at a relative blockade depth ratio $\langle i\rangle/\langle i_0\rangle \approx 0.16$ (fig. 4(A)), perhaps representing all of the putative $[PW_{11}O_{39}]^{7-}$ subspecies in the pore. However, at $V = -100\,$mV and $-80\,$mV (figs. 4(B) and (C), respectively), this major peak shifts to a deeper relative current blockade levels and is split. The latter suggests that fewer of those subspecies partition into the pore. Note that these narrower peaks are still wider than those obtained with the PEG29 control (fig. 4(D)). Under these conditions, decreasing the magnitude of the applied potential further does not yield a further split, because the POM-induced current blockades are persistent and not removed until the applied potential is reversed (*data not shown*). Interestingly, increasing the electrolyte concentration to 3 M NaCl reduced the tendency of POMs to persistently block the pore at lower potentials (see fig. 5(A)), but further separation within the major peak is still not achieved even with potentials as low as $V = -40\,$mV. However, the full width at half maximum of the blockade depth histograms decreases by a factor of two when the magnitude of the applied potential decreases from $-80\,$mV to $-40\,$mV (data not shown). This is consistent with the notion that a greater concentration of NaCl would shift the equilibrium to fewer subspecies of $[PW_{11}O_{39}]^{7-}$ present and thus the number of them available to be driven into the pore, which would result in a narrower major peak in the nanopore current blockade histogram.

We reasoned that if the residence time of POMs in a nanopore were longer-lived, it might be easier to identify the possibly different species within the major peak in figs. 4(A)–(C). It is known that the residence times of peptides [43–45], sugars [46,47], unfolded proteins [48–51], PEGs [52], and oligonucleotides [53] are up to several orders of magnitude longer in the aerolysin nanopore than they are in the αHL channel. The question was whether this would also be the case for POMs.

POMs added to the 3 M NaCl electrolyte solution on the *cis* side of either the αHL (fig. 5(A)) or aerolysin channel (fig. 5(B)) caused ionic current blockades. At 40 mV applied potential and the same POM concentration, the capture rate of POMs by the aerolysin channel is several-fold less than that obtained with the αHL channel, presumably because aerolysin's pore diameter is less than that of αHL. Figure 5(C) shows that the mean residence time of POMs in the aerolysin channel (red circles) is similar to that obtained with the αHL nanopore (blue triangles), *i.e.*, $310\,\mu$s *vs.* $400\,\mu$s, respectively. Thus, aerolysin provides no significant advantage to further separate the putatively different species of $[PW_{11}O_{39}]^{7-}$ described above for fig. 4(C).

Conclusions

The ability to optimally detect, characterize, and identify individual molecules with nanopores depends critically on understanding the physical and chemical nature

of the ionic current blockade signals they cause. To address this metrology issue, and advance the use of single-molecule nanopore-based sensing as an analytical tool, we developed a theory that fully accounts for the interactions between flexible PEG polymers, cations, and the αHL nanopore over a wide range of polymer size [15]. That theory, which accurately and precisely identifies differently sized PEG polymers based on their conductance blockade depths and residence times in the αHL nanopore [15,36] qualitatively accounts for single-molecule–induced current blockades in other protein and in solid-state nanopores. However, while detection and separation of rigid metallonanoparticles is possible by this method, it is clear that the partitioning behavior of this class of compounds requires further experimental and theoretical work to develop the methods and models further to achieve full separation and identification of different subspecies. It is likely that studying other metallonanoparticles of different composition and with known amounts of fixed charges will shed light on this issue.

This work was supported in part by the National Institutes of Health NHGRI (Grant R01 HG007415) and China Postdoctoral Science Foundation (Grant 2014 M560670). Pre-formed wild-type αHL heptamer was a kind gift from Drs. Sergey Kalachikov and Jingyue Ju at Columbia University. We thank Drs. Donald Atha and John Henry at NIST for fruitful discussions on the manuscript. The identification of commercial materials and their sources is given to describe the experimental results. In no case does this identification imply recommendation by the National Institute of Standards and Technology, nor does it imply that the materials are the best available.

Author contribution statement

Haiyan Wang performed some of the experiments, analyzed some of the data, and edited the manuscript. Joseph W.F. Robertson analyzed some of the data, prepared some of the figures, and edited the manuscript. Dianne L. Poster edited the manuscript. John J. Kasianowicz wrote the manuscript, and analyzed some of the data. Jessica Ettedgui conceived the project, performed some of the experiments, analyzed some of the data, and edited the manuscript.

References

1. B. Katz, *Nerve, Muscle, and Synapse* (New York, McGraw-Hill, 1966).
2. B. Hille, *Ion Channels of Excitable Membranes*, 3rd ed. (Sunderland, MA, 2001).
3. A.L. Harris, Q. Rev. Biophys. **34**, 325 (2002).
4. J.J. Kasianowicz, J.W.F. Robertson, E.R. Chan, J.E. Reiner, V.M. Stanford, Annu. Rev. Anal. Chem. **1**, 737 (2008).
5. S. Bezrukov, J.J. Kasianowicz, Phys. Rev. Lett. **70**, 2352 (1993).
6. J.J. Kasianowicz, S.M. Bezrukov, Biophys. J. **69**, 94 (1995).
7. J.J. Kasianowicz, D.L. Burden, L.C. Han, S. Cheley, H. Bayley, Biophys. J. **76**, 837 (1999).
8. J.J. Kasianowicz, E. Brandin, D. Branton, D. Deamer, Proc. Natl. Acad. Sci. U.S.A. **93**, 13770 (1996).
9. M. Akeson, D. Branton, J.J. Kasianowicz, E. Brandin, D. Deamer, Biophys. J. **77**, 3227 (1999).
10. O.V. Krasilnikov, R.Z. Sabirov, V.I. Ternovsky, P.G. Merzliak, J.N. Muratkhodjaev, FEMS Microbiol. Immun. **105**, 93 (1992).
11. S.M. Bezrukov, I. Vodyanoy, R. Brutyan, J.J. Kasianowicz, Macromolecules **29**, 8517 (1996).
12. L. Movileanu, H. Bayley, Proc. Natl. Acad. Sci. U.S.A. **98**, 10137 (2001).
13. O.V. Krasilnikov, *Sizing Channels with Neutral Polymers*, in *Structure and Dynamics of confined polymers, NATO Sci. Ser.*, Vol. **87** (Springer Netherlands, Dordrecht, 2002) pp. 97–115.
14. J.W.F. Robertson, C.G. Rodrigues, V.M. Stanford, K.A. Rubinson, O.V. Krasilnikov, J.J. Kasianowicz, Proc. Natl. Acad. Sci. U.S.A. **104**, 8207 (2007).
15. J.E. Reiner, J.J. Kasianowicz, B.J. Nablo, J.W.F. Robertson, Proc. Natl. Acad. Sci. U.S.A. **107**, 12080 (2010).
16. G. Baaken, N. Ankri, A.-K. Schuler, J. Rühe, J.C. Behrends, ACS Nano **5**, 8080 (2011).
17. A. Oukhaled, B. Cressiot, L. Bacri, M. Pastoriza-Gallego, J.-M. Betton, E. Bourhis, R. Jede, J. Gierak, L. Auvray, J. Pelta, ACS Nano **5**, 3628 (2011).
18. E.A. Manrao, I.M. Derrington, A.H. Laszlo, K.W. Langford, M.K. Hopper, N. Gillgren, M. Pavlenok, M. Niederweis, J.H. Gundlach, Nat. Biotechnol. **30**, 349 (2012).
19. S. Kumar, C. Tao, M. Chien, B. Hellner, A. Balijepalli, J.W.F. Robertson, Z. Li, J.J. Russo, J.E. Reiner, J.J. Kasianowicz, J. Ju, Sci. Rep. **2**, 684 (2012).
20. C.W. Fuller, S. Kumar, M. Porel, M. Chien, A. Bibillo, P.B. Stranges, M. Dorwart, C. Tao, Z. Li, W. Guo, S. Shi, D. Korenblum, A. Trans, A. Aguirre, E. Liu, E.T. Harada, J. Pollard, A. Bhat, C. Cech, A. Yang, C. Arnold, M. Palla, J. Hovis, R. Chen, I. Morozova, S. Kalachikov, J.J. Russo, J.J. Kasianowicz, R. Davis, S. Roever, G.M. Church, J. Ju, Proc. Natl. Acad. Sci. U.S.A. **113**, 5233 (2016).
21. S.E. Henrickson, E. DiMarzio, Q. Wang, V.M. Stanford, J.J. Kasianowicz, J. Chem. Phys. **132**, 135101 (2010).
22. J.J. Kasianowicz, S.E. Henrickson, H.H. Weetall, B. Robertson, Anal. Chem. **73**, 2268 (2001).
23. W. Vercoutere, S. Winters-Hilt, H. Olsen, D. Deamer, D. Haussler, M. Akeson, Nat. Biotechnol. **19**, 248 (2001).
24. O.K. Dudko, J. Mathe, A. Szabo, A. Meller, G. Hummer, Biophys. J. **92**, 4188 (2007).
25. J.J. Kasianowicz, J.E. Reiner, J.W.F. Robertson, S.E. Henrickson, C. Rodrigues, O.V. Krasilnikov, *Detecting and characterizing individual molecules with single nanopores*, in *Nanopore-Based Technology, Methods in Molecular Biology*, edited by M. Gracheva, Vol. **870** (Totowa, NJ: Humana Press, 2012) pp. 3–20.
26. M. Pope, *Heteropoly and Isopoly Oxometalates* (Springer, 2013).

27. A. Bijelic, A. Rompel, Coord. Chem. Rev. **299**, 22 (2015).
28. J. Ettedgui, J.J. Kasianowicz, A. Balijepalli, J. Am. Chem. Soc. **138**, 7228 (2016).
29. H.S. White, A. Bund, Langmuir **24**, 2212 (2008).
30. S.P. Howard, W.J. Garland, M.J. Green, J.T. Buckley, J. Bacteriol. **169**, 2869 (1987).
31. J.T. Buckley, S.P. Howard, Methods Enzymol. **165**, 193 (1988).
32. J.T. Buckley, S.P. Howard, Infect. Immun. **67**, 466 (1999).
33. M.W. Parker, J.T. Buckley, J.P. Postma, A.D. Tucker, K. Leonard, F. Pattus, D. Tsernoglou, Nature **367**, 292 (1994).
34. J.M. del Rio Martinez, E. Zaitseva, S. Petersen, G. Baaken, J.C. Behrends, Small **11**, 119 (2015).
35. C.G. Rodrigues, D.C. Machado, S.F. Chevtchenko, O.V. Krasilnikov, Biophys. J. **95**, 5186 (2008).
36. A. Balijepalli, J.W.F. Robertson, J.E. Reiner, J.J. Kasianowicz, R.W. Pastor, J. Am. Chem. Soc. **135**, 7064 (2013).
37. A. Balijepalli, J. Ettedgui, A.T. Cornio, J.W.F. Robertson, K.P. Cheung, J.J. Kasianowicz, C. Vaz, ACS Nano **8**, 1547 (2014).
38. W. Junge, S. McLaughlin, Biochim. Biophys. Acta **890**, 1 (1987).
39. W.H. Knoth, R.L. Harlow, J. Am. Chem. Soc. **103**, 1865 (1981).
40. M.A. Fedotov, R.I. Maksimovskaya, J. Struct. Chem. **47**, 952 (2006).
41. E.C. Yusko, J.M. Johnson, S. Majd, P. Prangkio, R.C. Rollings, J. Li, J. Yang, M. Mayer, Nat. Nanotechnol. **6**, 253 (2011).
42. H. Wang, J. Ettedgui, J. Forstater, J.W.F. Robertson, J.E. Reiner, H. Zhang, S. Chen, J.J. Kasianowicz, ACS Sens. **3**, 251 (2018).
43. R. Stefureac, Y.-T. Long, H.-B. Kraatz, P. Howard, J.S. Lee, Biochemistry **45**, 9172 (2006).
44. Y. Wang, V. Montana, V. Grubišić, R.F. Stout, V. Parpura, L.-Q. Gu, ACS Appl. Mater. Interfaces **7**, 184 (2015).
45. F. Piguet, H. Ouldali, M. Pastoriza-Gallego, P. Manivet, J. Pelta, A. Oukhaled, Nat. Commun. **9**, 966 (2018).
46. L. Bacri, A. Oukhaled, E. Hémon, F.B. Bassafoula, L. Auvray, R. Daniel, Biochem. Biophys. Res. Commun. **412**, 561 (2011).
47. A. Fennouri, C. Przybylski, M. Pastoriza-Gallego, L. Bacri, L. Auvray, R. Daniel, ACS Nano **6**, 9672 (2012).
48. M. Pastoriza-Gallego, L. Rabah, G. Gibrat, B. Thiebot, F.G. van der Goot, L. Auvray, J.-M. Betton, J. Pelta, J. Am. Chem. Soc. **133**, 2923 (2011).
49. C. Merstorf, B. Cressiot, M. Pastoriza-Gallego, A. Oukhaled, J.-M. Betton, L. Auvray, J. Pelta, ACS Chem. Biol. **7**, 652 (2012).
50. L. Payet, M. Martinho, M. Pastoriza-Gallego, J.-M. Betton, L. Auvray, J. Pelta, J. Mathe, Anal. Chem. **84**, 4071 (2012).
51. M. Pastoriza-Gallego, M.-F. Breton, F. Discala, L. Auvray, J.-M. Betton, J. Pelta, ACS Nano **8**, 11350 (2014).
52. G. Baaken, I. Halimeh, L. Bacri, J. Pelta, A. Oukhaled, J.C. Behrends, ACS Nano **9**, 6443 (2015).
53. C. Cao, Y.-L. Ying, Z.-L. Hu, D.-F. Liao, H. Tian, Y.-T. Long, Nat. Nanotechnol. **11**, 713 (2016).